A New Four Quadrant Field Orientation-Controlled Three-Phase Induction Motor Drive Based on Hysteresis Current Comparison

Cosmas Uchenna OGBUKA, Cajethan Maduabuchi NWOSU, Marcel Ugwoke AGU

Department of Electrical Engineering, Faculty of Engineering,
University of Nigeria, Nsukka Road, 410001 Nsukka, Nigeria

cosmas.ogbuka@unn.edu.ng, cajethan.nwosu@unn.edu.ng, marcel.agu@unn.edu.ng

DOI: 10.15598/aeee.v15i2.2128

Abstract. *A new four quadrant Field Orientation-Controlled (FOC) three-phase induction motor drive based on Hysteresis Current Comparison (HCC) has been developed. The direct relationship between current and torque in the Direct-Quadrature (dq) reference frames has been exploited to develop an HCC scheme that offers accurate tracking of current and torque based on the pulse width modulation technique. The parameters of the inner HCC and the outer Proportional-Integral (PI) speed controllers have been optimised to obtain effective current and torque tracking. The complete closed loop system being speed-controlled, four quadrant operation has been obtained using step speed input while the suitability of the developed model has been tested under full load stress during steady state. The results obtained satisfy the four quadrant operation requirements of advanced drives where controlled starts and stops are essential in both forward and reverse directions. This is evident in the effectiveness of current and torque tracking and ease of speed transition from motoring to regeneration and vice versa. The developed model finds applications in advanced industrial drives as an energy-efficient and cost-effective alternative to eliminate the effects of supply voltage drops and mechanical load variations.*

Keywords

Field orientation, four quadrant, Hysteresis Current Control, induction motor.

1. Introduction

The induction machine, particularly with squirrel cage, is the most commonly used machine in AC drives being very economical, rugged and reliable [1], [2], [3], [4], [5] and [6]. Advances in power electronic devices and fast digital processors have provided the possibility of achieving high performance drives; even in four quadrants to satisfy the requirements of advanced drives [7] and [8].

Four quadrant drives offer the opportunity for the utilization of induction motor drives in high dynamic applications where controlled starts and stops are required. If a machine is required to be brought to rest from steady state, instead of abrupt supply interruption with its attendant hazards, the machine can be made to work as a generator thereby the stored kinetic energy can be effectively transferred to the source. This saves energy and brings the machine to rest rapidly and safely. To make a machine transit from motoring to generating mode, power flow is reversed from the machine to the power supply source. This is called regenerative braking. The braking is accomplished by regeneration implying that a negative torque is generated in the machine as opposed to positive motoring torque [9], [10], [11], [12], [13], [14], and [15]. The Tab. 1 summarises the four quadrant operation modes where '+' and '−' represent positive and negative respectively.

Figure 1 illustrates the torque-speed profile in four quadrant drives. A mirror image of the torque speed characteristics of quadrant I is obtained in quadrant IV. The quadrant I and IV represent forward motoring and forward regenerating respectively in the forward direction. Some applications require operation in both

Tab. 1: Four quadrant operation modes.

Mode	Quadrant	Speed	Torque	Power Output
Forward Motoring (FM)	I	+	+	+
Forward Regenerating (FR)	IV	+	−	−
Reverse Motoring (RM)	III	−	−	+
Reverse Regenerating (RR)	II	−	+	−

$$\begin{bmatrix} v_{ds} \\ v_{qs} \\ 0 \\ 0 \end{bmatrix} = \begin{bmatrix} R_s + pL_s & -\omega_e L_s & pL_m & -\omega_e L_m \\ \omega_e L_s & R_s + pL_s & \omega_e L_m & pL_m \\ pL_m & -\omega_{sl} L_m & R_r + pL_r & -\omega_{sl} L_r \\ \omega_{sl} L_m & pL_m & \omega_{sl} L_r & R_r + pL_r \end{bmatrix} \cdot \begin{bmatrix} i_{ds} \\ i_{qs} \\ i_{dr} \\ i_{qr} \end{bmatrix}. \tag{1}$$

forward and reverse directions. In such cases, quadrant III and quadrant II represent reverse motoring and reverse regenerating respectively.

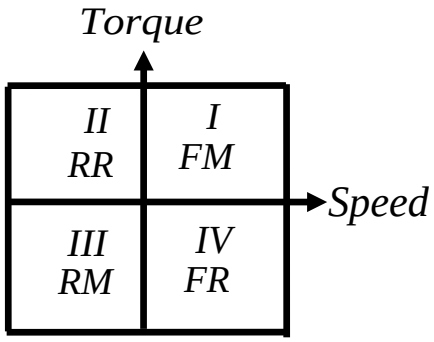

Fig. 1: Torque-speed profile in four quadrant drives.

Due to the direct proportionality of current and torque, current control strategies are employed in Adjustable Speed Drives (ASD) to ensure that stator currents track their respective reference values. Prominent among the current control strategies is the HCC due to ease of implementation, excellent transient response, attainment of maximum current limit and insensitiveness to load parameter variations [16], [17], [18], [19] and [20]. The developed HCC is a three-phase Pulse Width Modulation technique and is suitable for a variety of industrial applications such as variable speed electric motor drives, uninterruptible power system, active power filters, and more recently, in renewable energy conversion systems and hybrid vehicles [21].

In this work, a new four-quadrant Field Orientation-Control (FOC) of three-phase induction motor drive based on Hysteresis Current Comparison (HCC) is presented. The parameters of both the outer PI speed controller and the inner HCC of the complete closed loop speed-controlled system are optimised to obtain optimum performance using four-quadrant step speed input simultaneously with full load stress at designated points during steady state to determine the suitability of the developed speed-controlled system for four-quadrant operation. The simulation environment is MATLAB/Simulink software 2014 version.

2. Model of Three-Phase Induction Motor for Field Orientation Control

The dynamic voltage equations of the squirrel cage induction motor in the synchronously rotating reference frame is shown in Eq. (1) [22] and [23].

The electromagnetic torque and rotor dynamic equations are shown in Eq. (2) and Eq. (3) respectively.

$$T_e = \frac{3}{2}\frac{P}{2}\frac{L_m}{L_r}\left(\Psi_{dr} i_{qs} - \Psi_{qr} i_{ds}\right), \tag{2}$$

$$T_e = T_L + B\omega_r + Jp\omega_r, \tag{3}$$

where v_{ds}, v_{qs} - d, q-axis stator voltages; R_s, R_r - stator, rotor resistances; L_s, L_r, L_m - stator, rotor, magnetizing inductances; L_{lr}, L_{ls} - rotor, stator leakage inductances; $L_r = L_{lr} + L_m$, $L_s = L_{ls} + L_m$, $\omega_r, \omega_e, \omega_{sl}$ - rotor, synchronous, slip speeds; P - number of poles; $\omega_{sl} = \omega_e - \frac{P}{2}\omega_r$; Ψ_{dr}, Ψ_{qr} - d, q-axis rotor flux linkages, p - differential operator; T_e - electromagnetic torque; T_L- load torque; B - rotor damping coefficient; J - inertia constant.

The FOC controls the stator current vector of the induction machine to achieve a precise and independent control of torque and flux as obtainable in the DC machines. The stator current vector contains the torque controlling component, i_{qs}, and the flux controlling component, i_{ds} as shown in the phasor diagram of Fig. 2.

From Fig. 2, field orientation is feasible because the entire rotor flux Ψ_r is aligned to the d-axis thereby making the q-axis flux component Ψ_{qr} zero since they are perpendicular to each other. Consequently, Eq. (2) reduces to Eq. (4) where $T_e \propto i_{qs}$. Also, from the rotor flux orientation described above, Eq. (5) shows that the rotor flux $\Psi_r \propto i_{ds}$.

$$T_e = \frac{3}{2}\frac{P}{2}\frac{L_m}{L_r}\Psi_{dr} i_{qs}. \tag{4}$$

$$\Psi_r = \Psi_{dr} = L_m i_{ds}. \tag{5}$$

Under this condition, the induction motor behaves exactly as the separately excited DC motor where the q-axis stator current i_{qs} entirely controls the electromagnetic torque and the d-axis stator current i_{ds} entirely controls rotor flux.

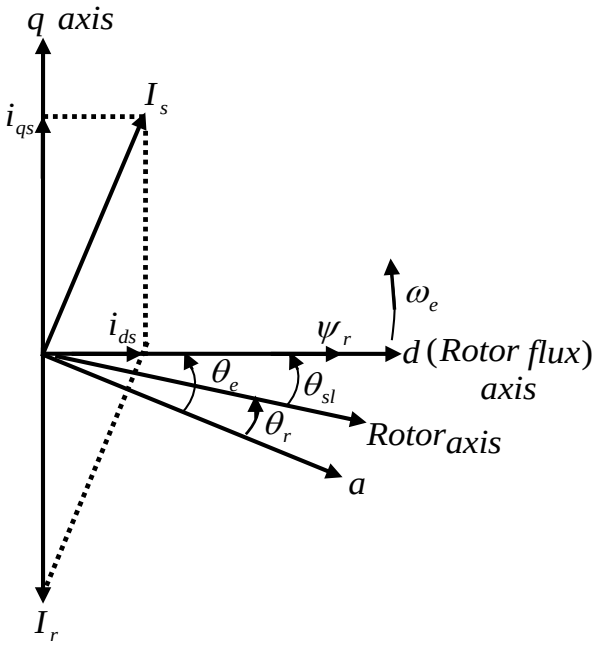

Fig. 2: Phasor diagram of FOC for induction motor.

3. Complete Schematic of the Speed-Controlled Drives System

The induction motor in the scheme of Fig. 3 is fed by an HCC PWM inverter operating as a three-phase sinusoidal current source.

The rotor speed ω_r is measured by the speed sensor and filtered by the 1st order low pass filter. The speed error between the actual rotor speed and its reference is processed through the Proportional-Integral (PI) speed controller to nullify the steady state error in speed. The output is restricted to an upper and a lower limit to produce a realistic reference torque T_e^*. The Fig. 4 shows the realisation of the reference phase currents as expressed from Eq. (6) to Eq. (16). All reference or command values are superscripted with * in the diagrams.

$$i_{ds}^* = \frac{|\Psi_r|^*}{L_m}. \tag{6}$$

$$\Psi_r = \frac{L_m i_{ds}}{1 + \tau_r s}, \tag{7}$$

where $\tau_r = \frac{L_r}{R_r}$ is the rotor time constant.

$$i_{qs}^* = \frac{2}{3}\frac{2}{P}\frac{L_r}{L_m}\frac{T_e^*}{\Psi_r}. \tag{8}$$

$$i_s^* = \sqrt{i_{ds}^* + i_{qs}^*}. \tag{9}$$

$$\omega_{sl} = \frac{L_m}{\Psi_r}\frac{R_r}{L_r} i_{qs}. \tag{10}$$

$$\theta_e = \int \left(\frac{P}{2}\omega_r + \omega_{sl}\right) \mathrm{d}t. \tag{11}$$

$$i_{qs} = \frac{2}{3}\left(i_a \cos\theta_e + i_b \cos\left(\theta_e - \frac{2\pi}{3}\right) + \right. \\ \left. + i_c \cos\left(\theta_e + \frac{2\pi}{3}\right)\right). \tag{12}$$

$$i_{ds} = \frac{2}{3}\left(i_a \sin\theta_e + i_b \sin\left(\theta_e - \frac{2\pi}{3}\right) + \right. \\ \left. + i_c \sin\left(\theta_e + \frac{2\pi}{3}\right)\right). \tag{13}$$

The reference phase currents are computed using the inverse park's transform as:

$$i_a^* = i_{qs}^* \cos\theta_e + i_{ds}^* \sin\theta_e. \tag{14}$$

$$i_b^* = i_{qs}^* \cos\left(\theta_e - \frac{2\pi}{3}\right) + i_{ds}^* \sin\left(\theta_e - \frac{2\pi}{3}\right). \tag{15}$$

$$i_c^* = i_{qs}^* \cos\left(\theta_e + \frac{2\pi}{3}\right) + i_{ds}^* \sin\left(\theta_e + \frac{2\pi}{3}\right). \tag{16}$$

The reference phase currents (i_a^*, i_b^*, and i_c^*) and the corresponding actual phase currents (i_a, i_b, and i_c), obtained by feedback, are compared using the control logic shown below:

Algorithm 1

IF $i_{a,b,c} < i_{a,b,c}^* - \Delta i_s^*$ **OR** $\left(i_{(a,b,c)} > i_{(a,b,c)}^* - \Delta i_s^*$ **AND** $i_{(a,b,c)} < i_{(a,b,c)}^* + i_s^*$ **AND** $\frac{\mathrm{d}i_{(a,b,c)}}{\mathrm{d}t} > 0\right)$
THEN $v_{g(1,3,5)} = 1$, $v_{g(4,6,2)} = 0$
ELSE $v_{g(1,3,5)} = 0$, $v_{g(4,6,2)} = 1$
END

From the control logic shown above, it is seen that error signals are generated and used to generate the voltage gating signals for the switches of the Three-Phase (3ϕ) IGBT Voltage Source Inverter (VSI). The

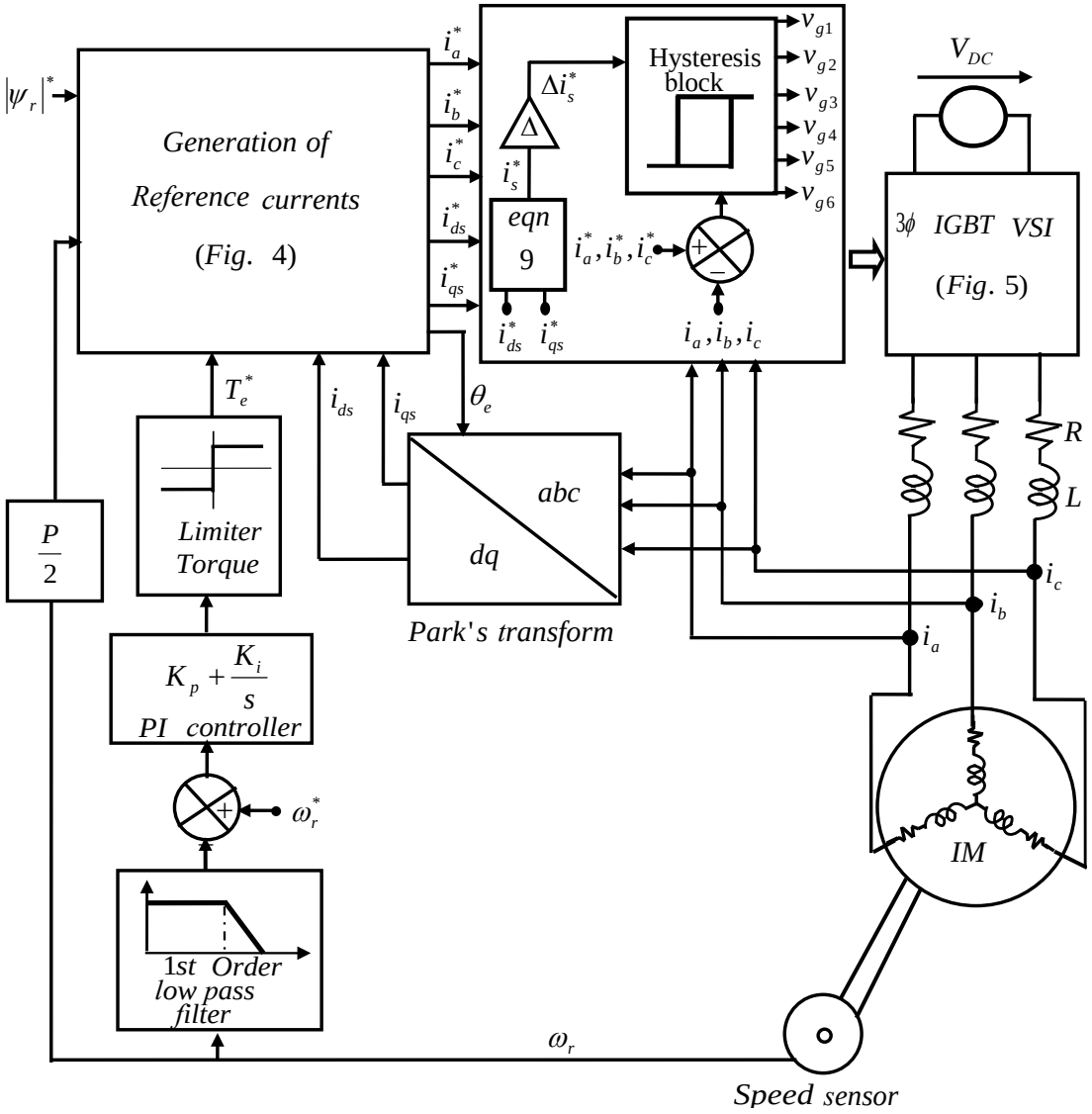

Fig. 3: Complete schematic of the speed-controlled induction motor drive system.

HCC action is made possible by Δi_s^*, where Δ, which is between 0 and 1 ($0 < \Delta < 1$), is an adjustable hysteresis window which determines the effectiveness of current and torque tracking [24].

Current control is achieved by the appropriate firing of the power semiconductor switches S_1 to S_6 of the three-phase inverter. The inverter is supplied by an adequately filtered DC source V_{dc}. Each phase current to the motor is limited by the series RL branch (R =0.001 Ω and L = 5 mH).

4. Results and Discussions

The appendix A shows the parameters of the three-phase induction motor under study. The complete drive system is simulated for a four-quadrant operation from 500 rpm to 500 rpm to 500 rpm and the results presented and discussed. Best performance was obtained by the appropriate tuning of the controller variables as is the practice in industry. The optimal control variables are: Proportional gain = 5, Integral gain = 100, 1st Order Low Pass Filter Time Constant = $1.6 \cdot 10^{-3}$ seconds, Torque Limiter Upper Lower = 75 Nm/−75 Nm, Hysteresis Band $\Delta = 0.05$.

The HCC property that determines the inverter switching is shown in Fig. 6 for time range 0.2936 to 0.2938 seconds using phase 'a' for illustration. Similar behaviours are obtained for phases 'b' and 'c'. The phase 'a' current i_a tracts the upper boundary $i_a^* + \Delta i_s^*$ (increases) when switch S_1 is conducting and tracts the lower boundary $i_a^* - \Delta i_s^*$ (decreases) when switch S_4 is conducting. The Hysteresis Current Control action, which makes i_a to track its reference i_a^*, is seen as i_a

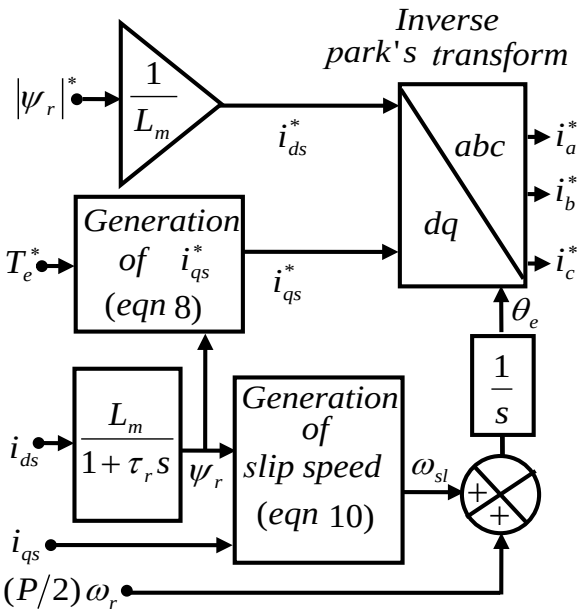

Fig. 4: Generation of reference phase currents.

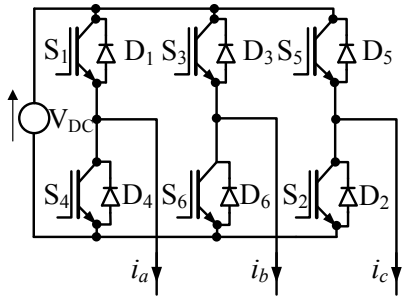

Fig. 5: Power circuit of three-phase IGBT VSI.

moves between $i^*_a + \Delta i^*_s$ to $i^*_a - \Delta i^*_s$ as switches S_1 and S_4 conduct alternately. The narrower the hysteresis band δ, the more accurately the actual current i_a tracts the reference current i_a. Smaller hysteresis bands imply higher switching frequency and vice versa. This may constitute a practical limitation on the power device switching capability due to switching losses, which need to be mitigated.

On no load, a reference speed of 500 rpm is applied until 0.4 seconds when a speed command of −500 rpm is made, followed by a step up to 500 rpm at 0.8 seconds to complete a drive in four quadrants as shown in Fig. 7. The rotor position remained on the increase for as long as the motor speed is positive (Forward Motoring, FM and Forward Regeneration, FR). As soon as the rotor speed becomes negative, the rotor position reverses orientation (Reverse Motoring, RM and Reverse Regeneration, RR).

At steady state during reverse motoring, full load step input is applied and removed at 0.65 seconds and

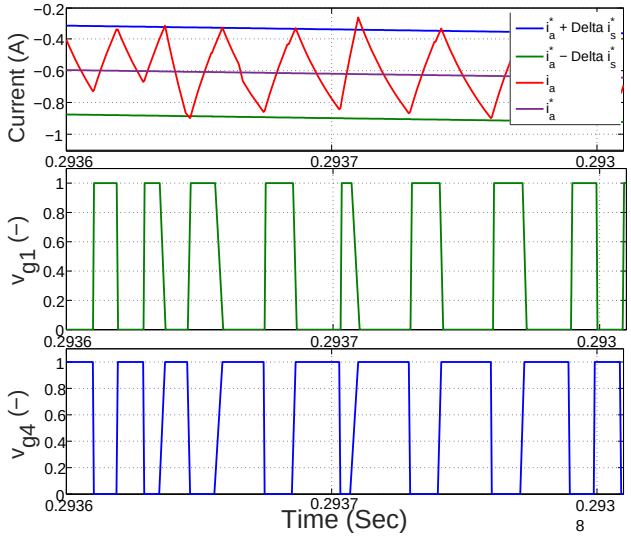

Fig. 6: Hysteresis current and gating signals for phase A.

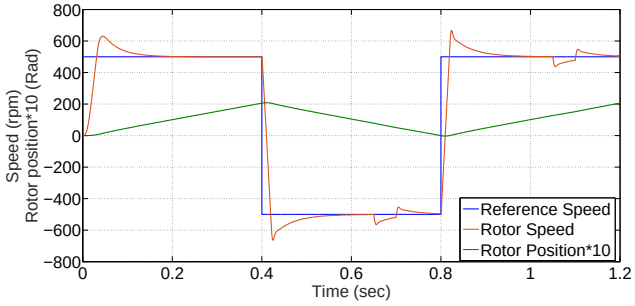

Fig. 7: Reference speed, rotor speed and rotor position.

0.7 seconds respectively as shown in Fig. 8. It is also repeated during forward motoring at 1.05 seconds and 1.1 seconds respectively. The effect of sudden gain and loss of load is evident in the rotor speed and on the phase currents.

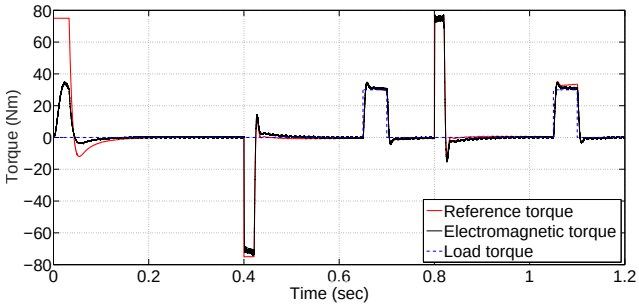

Fig. 8: Reference torque, electromagnetic torque and load torque.

Comparing Fig. 9 and Fig. 10, the actual phase current accurately tracts the reference both during transient disturbances and steady state condition. The switching period, is seen from the current waveforms, to be the same both for positive speed of 500 rpm and negative speed of −500 rpm.

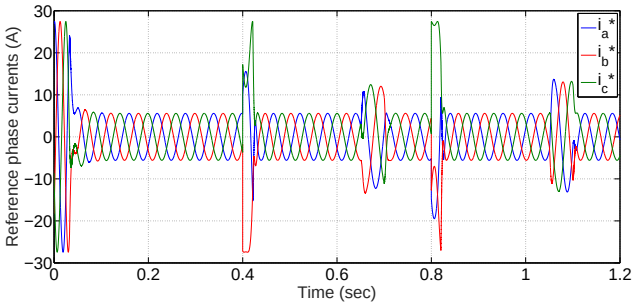

Fig. 9: Reference phase currents.

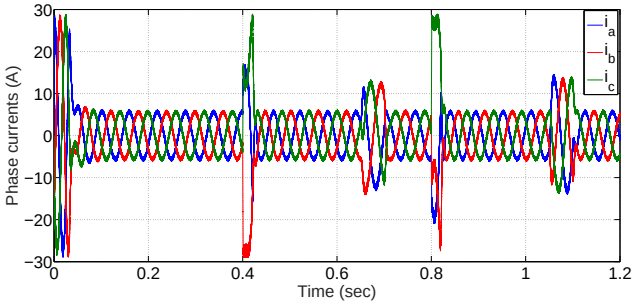

Fig. 10: Actual phase currents.

Motor response in all four possible modes of operation namely Forward Motoring (FM), Forward Regeneration (FR), Reverse Motoring (RM) and Reverse Regeneration (RR) are obtained as shown in the Torque-Speed profile of Fig. 11.

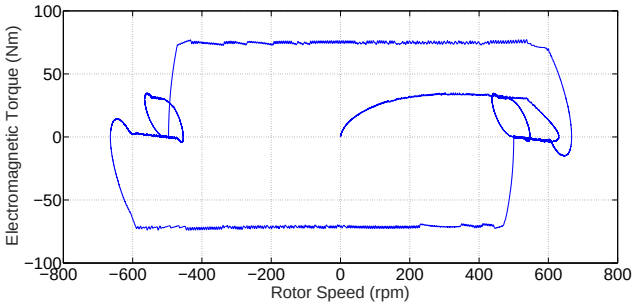

Fig. 11: Four quadrant torque speed profile.

5. Conclusion

A new four quadrant field orientation-controlled three-phase induction motor drive based on Hysteresis Current Comparison (HCC) has been successfully realised. By applying step transition in speed and full stress step loading, motor operation in all the four possible quadrants of operation namely Forward Motoring (FM), Forward Regeneration (FR), Reverse Motoring (RM) and Reverse Regeneration (RR) was obtained. This is what obtains in numerous applications in industry where controlled starts and stops are required in both forward and reverse directions. Dynamic braking occasioned by regeneration in both the forward and reverse direction proves to be a better mean of stopping the motor rather than the usually hazardous option of supply interruption. The controller variables of the developed speed-controlled drives system were optimised to obtain optimal drives performance. The results presented show that the developed HCC algorithm offered excellent dynamic response and steady state performance necessary in advanced motor drives.

Acknowledgment

The authors kindly wish to acknowledge the Murli T. Chalaram Foundation (MTC) for the postgraduate fee scholarship offered to the first author for his doctoral research studies during which this research was conducted.

References

[1] UDDIN, M. N. and H. WEN. Development of a Self-Tuned Neuro-Fuzzy Controller for Induction Motor Drives. *IEEE Transactions on Industry Applications*. 2007, vol. 43, iss. 4, pp. 1108–1116. ISSN 1939-9367. DOI: 10.1109/TIA.2007.900472.

[2] BOSE, B. K. Power electronics and motion control-technology status and recent trends. *IEEE Transaction on Industry Applications*. 1993, vol. 29, no. 5, pp. 902–909. ISSN 1939-9367. DOI: 10.1109/28.245713.

[3] BOCKER, J. State of the Art of Induction Motor Control. In: *IEEE International Electric Machines & Drives Conference (IEMDC 07)*. Antalya: IEEE, 2007, pp. 1459–1464. ISBN 1-4244-0742-7. DOI: 10.1109/IEMDC.2007.383643.

[4] PETER, J., G. D. MARQUES and R. RAMCHAND. Current error space vector based constant switching frequency hysteresis controller for VSI fed Induction Motor drives. In: *9th International Conference on Compatibility and Power Electronics (CPE)*. Costa da Caparica: IEEE, 2015, pp. 246–251. ISBN 978-1-4799-6301-0. DOI: 10.1109/CPE.2015.7231081.

[5] HUANG, C.-Y., C.-P. WEI, J.-T. YU and Y.-J. HU. Torque and current control of induction motor drives for inverter switching frequency reduction. *IEEE Transactions on Industrial Electronics*. 2005, vol. 52, iss. 5, pp. 1364–1371. ISSN 1557-9948. DOI: 10.1109/TIE.2005.855660.

[6] VERMA, R., V. VERMA and C. CHAKRABORTY. ANN based sensorless vector controlled induction motor drive suitable for four quadrant operation. In: *IEEE Students' Technology Symposium (TechSym)*. Kharagpur: IEEE, 2014, pp. 182–187. ISBN 978-1-4799-2608-4. DOI: 10.1109/TechSym.2014.6808043.

[7] EL-KHOLY, E. E. High-Performance Induction Motor Drive Based on Adaptive Variable Structure Control. *Journal of Electrical Engineering*. 2005, vol. 56, no. 3–4, pp. 64–70. ISSN 1335-3632.

[8] TEJA, A. V. R. and C. CHAKRABORTY. A New Model Reference Adaptive Controller for Four Quadrant Vector Controlled Induction Motor Drives. *IEEE Transactions on Industrial Electronics*. 2012, vol. 59, iss. 10, pp. 3757–3767. ISSN 1557-9948. DOI: 10.1109/TIE.2011.2164769.

[9] AYDOGMUS, O. and S. SUNTER. Four-quadrant operation of PMSM drive fed by a matrix converter. In: *International Aegean Conference on Electrical Machines and Power Electronics and 2011 Electromotion Joint Conference (ACEMP)*. Istanbul: IEEE, 2011, pp. 436–439. ISBN 978-1-4673-5002-0. DOI: 10.1109/ACEMP.2011.6490638.

[10] HOSSAIN, S., I. HUSAIN, H. KLODE, B. LEQUESNE and A. OMEKANDA. In: *Seventeenth Annual IEEE Applied Power Electronics Conference and Exposition (APEC)*. Dallas: IEEE, 2011, pp. 41–47. ISBN 0-7803-7404-5. DOI: 10.1109/APEC.2002.989225.

[11] JOICE, C. S., S. R. PARANJOTHI and V. J. S. KUMAR. Digital Control Strategy for Four Quadrant Operation of Three Phase BLDC Motor With Load Variations. *IEEE Transactions on Industrial Informatics*. 2012, vol. 9, iss. 2, pp. 974–982. ISSN 1941-0050. DOI: 10.1109/TII.2012.2221721.

[12] VINATHA, U., S. POLA and K. VITTAL. Simulation of four quadrant operation & speed control of BLDC motor on MATLAB/SIMULINK. In: *IEEE Region 10 Conference (TENCON)*. Hyderabad: IEEE, 2008, pp. 1–6. ISBN 978-1-4244-2408-5. DOI: 10.1109/TENCON.2008.4766449.

[13] CHING, T. W. Four-quadrant Zero-current-transition Converter-fed Dc Motor Drives for Electric Propulsion. *Journal of Asian Electric Vehicles*. 2006, vol. 4, no. 2, pp. 911–917. ISSN 1348-3927. DOI: 10.4130/jaev.4.911.

[14] HUSAIN, I. and S. A. HOSSAIN. Modeling, Simulation, and control of switched reluctance motor drives. *IEEE Transactions on Industrial Electronics*. 2005, vol. 52, iss. 6, pp. 1625–1634. ISSN 1557-9948. DOI: 10.1109/TIE.2005.858710.

[15] KUMAR, M. S., P. R. BABU and S. RAMPRASATH. Four quadrant comparative evaluation of classical and space vector PWM-directtorque control of a VSI fed three phase induction motor drive in MATLAB/SIMULINK environment. In: *IEEE International Conference on Power Electronics, Drives and Energy Systems (PEDES)*. Bengaluru: IEEE, 2012, pp. 1–6. ISBN 978-1-4673-4508-8. DOI: 10.1109/PEDES.2012.6484467

[16] KAZMIERKOWSKI, M. P. and L. MALESANI. Current control techniques for three-phase voltage-source PWM converters: a survey. *IEEE Transactions on Industrial Electronics*. 1998, vol. 45, iss. 5, pp. 691–703. ISSN 1557-9948. DOI: 10.1109/41.720325.

[17] HOLTZ, J. Pulsewidth modulation-a survey. *IEEE Transactions on Industrial Electronics*. 1992, vol. 39, iss. 5, pp. 410–420. ISSN 1557-9948. DOI: 10.1109/41.161472.

[18] MAO, H., X. YANG, Z. CHEN and Z. WANG. A Hysteresis Current Controller for Single-Phase Three-Level Voltage Source Inverters. *IEEE Transactions on Power Electronics*. 2012, vol. 27, iss. 7, pp. 3330–3339. ISSN 1941-0107. DOI: 10.1109/TPEL.2011.2181419.

[19] DEY, A., P. P. RAJEEVAN, R. RAMCHAND, K. MATHEW and K. GOPAKUMAR. A Space-Vector-Based Hysteresis Current Controller for a General n-Level Inverter-Fed Drive With Nearly Constant Switching Frequency Control. *IEEE Transactions on Industrial Electronics*. 2013, vol. 60, iss. 5, pp. 1989–1998. ISSN 1557-9948. DOI: 10.1109/TIE.2012.2200217.

[20] KENNEL, R., E. EL-KHOLY, S. MAHMOUD, A. EL-REFAEI and F. ELKADY. A simple high performance current control scheme for induction motor drives. In: *31st Annual Conference of IEEE Industrial Electronics Society (IECON)*. Raleigh: IEEE, 2005, pp. 1762–1767. ISBN 0-7803-9252-3. DOI: 10.1109/IECON.2005.1569172.

[21] NAGARAJAN, S. and N. RAJENDRAN. Comparison of Fault Diagnostics on Z-Source and Trans Z-Source Inverter Fed Induction Motor Drives. *Indian Journal of Science and Technology*. 2015, vol. 8, iss. 32, pp. 1–9. ISSN 0974-6846. DOI: 10.17485/ijst/2015/v8i32/87868.

[22] BOSE, B. K. *Modern Power Electronics and AC Drives*. 1st ed. New Jersey: Prentice-Hall, Inc., 2002. ISBN 0-13-016743-6.

[23] KRAUSE, P. C., O. WASYNCZUK and S. D. SUDHOFF. *Analysis of Electric Machinery*. 1st ed. New York: IEEE Press, 1995. ISBN 0-78-031101-9.

[24] OGBUKA, C., C. NWOSU and M. AGU. A Fast Hysteresis Current–Controlled Permanent Magnet Synchronous Motor Drive Based on Field Orientation. *Journal of Electrical Engineering*. 2016, vol. 67, iss. 2, pp. 69–77. ISSN 1335-3632. DOI: 10.1515/jee-2016-0011.

About Authors

Cosmas Uchenna OGBUKA was born in Umuna Nigeria on 1st April, 1981. He holds the following degrees from the Department of Electrical Engineering, University of Nigeria Nsukka, where he has attained the rank of Senior Lecturer: B.Eng. (First Class Honors), M.Eng. (Distinction) and Doctor of Philosopy Ph.D. obtained in 2004, 2009 and December 2014 respectively. His research interests are in Electrical Machines, Drives and Power Electronics. He is presently (Feb 2017 to May 2017) on the ETT Fellowship at the Massachusetts Institute of Technology, Cambridge Massachusetts under MISTI-AFRICA. He previously (Nov. 2015 to April 2016) undertook a postdoctoral research visit at the Chair of Electrical Drives and Actuators (EAA) Universität der Bundeswehr München Germany with Professor Dr.-Ing. Dieter Gerling.

Cajethan Maduabuchi NWOSU a Senior Lecturer, was born on 1st October 1967. He obtained the B.Eng, M.Eng, and Ph.D. Degrees in Electrical Engineering from the University of Nigeria, Nsukka in 1994, 2004, and 2015 respectively. His areas of research interest include power electronic converters, electrical drives and renewable energy technologies.

Marcel Ugwoke AGU born on 13th May 1947 in Ohebe-Dim Nigeria, obtained his B.Sc. in Electrical Engineering in 1974 in the University of Nigeria, Nsukka. He also received his M.A.Sc. and Ph.D. in 1978 and 1982 respectively in Power Electronics from the University of Toronto Canada. He is a Professor of Power Electronics in the Department of Electrical Engineering University of Nigeria, Nsukka. His research interests are in Power Electronics. He has published wide in reputable journals.

Appendix A
AC Drive Parameters

Tab. 2: Parameters of the three-phase induction motor.

Power rating (Hp)	5.4
Rated Line Voltage (V)	400
Rated Frequency (Hz)	50
Stator Resistance (ω)	1.405
Stator leakage inductance (H)	0.005839
Rotor Resistance Referred to Stator (ω)	1.395
Rotor Leakage Inductance Referred to the Stator (H)	0.005839
Mutual Inductance (H)	0.1722
No. of Poles (-)	4
Motor Inertia (Kg·m^2)	0.0131
Motor Friction Factor (-)	0.0002985
Direct Axis Rotor Flux (-)	0.96172
Speed (rpm)	1430
Full Load Torque T_L (Nm)	26.71